Can Cyclic Voltammetry at Microdisc Electrodes Be Approximately Described by One-Dimensional Diffusion?

John A. Alden, Francis Hutchinson, and Richard G. Compton*

Physical and Theoretical Chemistry Laboratory, Oxford University, South Parks Road, Oxford OX1 3QZ, United Kingdom

Received: July 31, 1996; In Final Form: November 11, 1996[⊗]

Fast scan cyclic voltammetry using microdisc electrodes is now widely employed for the study of the kinetics and mechanism of electrode processes. For convenience, it is common for experimentalists to interpret the results assuming that the disc can be treated as either a planar or a hemispherical electrode. Both approximations are available in the now widely adopted one-dimensional simulation package DigiSim which can simulate the cyclic voltammetric response of arbitrarily complex reaction mechanisms. This paper critically addresses the validity of this simplification. To this end, the application of the strongly implicit procedure (SIP) is developed to simulate transient processes at microdisc electrodes. The approach is validated by the simulation of chronoamperometric transients resulting from potential steps at microdisc electrodes; excellent agreement is obtained with analytical and other simulation methods. The simulation method is then used to model the cyclic voltammetric response of electrochemically reversible processes at microdisc electrodes. Corresponding simulations are reported for microhemisphere electrodes using the backwards implicit in time (BIT) method, allowing comparison between the two electrode geometries so that limitations of treating voltammetry at microdisc electrodes by approximation to a one-dimensional (hemispherical) diffusion problem can be quantified. Strong reservations are expressed about the approximation under *transient* conditions.

Introduction

During the past decade, voltammetry using microelectrodes—electrodes possessing at least one dimension of a size no more than the micron scale—has led to significant advances in diverse areas of electrochemistry.[1−3] Of their several unique properties, the unusually large rates of mass transport in comparison to electrodes of conventional sizes permits the kinetic interrogation of processes, both heterogeneous and homogeneous, which were previously outside the scope of measurement by voltammetric means. The use of microelectrodes for kinetic studies has recently been reviewed[3] and the feasibility demonstrated of accessing nanosecond time scales through the use of fast scan ($\leq 10^6$ V s^{-1}) cyclic voltammetry.[4,5]

The interpretation of microdisc cyclic voltammetry so as to permit mechanistic and kinetic deductions requires the solution of the appropriate mass transport equations with the inclusion of any relevant homogeneous and/or heterogeneous kinetics. This is a two-dimensional problem which is most generally accomplished by means of numerical simulations.[6−10] However, such approaches are challenging largely because of the grossly nonuniform current density which characterizes a microdisc electrode,[1−3] and a range of conformal maps and expanding grids have been proposed.[7,8,10,11] It has been demonstrated[12−14] under steady-state conditions that the diffusion-controlled current to a disc of radius r_{disc} is equivalent to that to a hemisphere of radius $2r_{disc}/\pi$. The simulation of microdisc problems has been simplified by the supposing this approximation to be adequate under transient conditions[3,15−16] despite the fact that simulations of potential steps[17] show this to be increasingly unsatisfactory at shorter times.[12] The popular commercial package DigiSim,[18,19] based on the FIFD simulation method of Rudolph,[20,21] permits any experimental electrochemist to simulate cyclic voltammetry for arbitrary mechanisms at planar and hemispherical electrodes regardless of their simulation skills. This paper therefore addresses the extent to which planar, and particularly hemispherical, microelectrodes can be used to approximate the cyclic voltammetric response of microdisc electrodes. First, we examine the case of an electrochemically reversible process for which approximate analytical treatments have appeared,[22] where the microdisc edge effects are most significant.[8] Second, we consider the simulation of electrode processes involving coupled homogeneous kinetics. Strong reservations are expressed about the hemisphere/disc approximation under transient conditions. Potential step transients are also considered to provide a check on the veracity of the simulation procedures.

Theory: Simulations

We consider the following electrochemically reversible process

$$A + e^- \equiv B \tag{1}$$

where A and B are both kinetically stable species and suppose throughout that only the former is present in bulk solution at a concentration $[A]_{bulk}$.

The time-dependent diffusion equation for transport to a microdisc electrode is

$$\frac{\partial a}{\partial t} = D\frac{\partial^2 a}{\partial z^2} + D\frac{\partial^2 a}{\partial r^2} + \frac{D}{r}\frac{\partial a}{\partial r} \tag{2}$$

where D is the diffusion coefficient (assumed equal for A and B), $a = [A]/[A]_{bulk}$, and the cylindrical coordinates r and z are defined in Figure 1. It is assumed that adequate supporting electrolyte is present to suppress migration effects. The corresponding transport equation for a hemisphere electrode is

$$\frac{\partial a}{\partial t} = D\frac{\partial^2 a}{\partial r^2} + \frac{2D}{r}\frac{\partial a}{\partial r} \tag{3}$$

where the coordinate r is defined in Figure 2.

* To whom correspondence should be addressed.

[⊗] Abstract published in *Advance ACS Abstracts,* January 1, 1997.

S1089-5647(96)02323-1 CCC: $14.00

In the following we examine, at both types of electrode, first the current transient resulting from a potential step between values at which no current flows and at which the current is transport limited. Second, we consider the current−potential dependence resulting from cyclic voltammetry. In this case the potential, $E(t)$, is scanned linearly with time, from a starting potential E_{init}, at a scan rate s.

$$E(t) = E_{init} + st \qquad t \le t_{scan} \tag{4a}$$

up to a time t_{scan} after which the direction of the scan is reversed.

$$E(t) = E_{init} + st_{scan} - s(t - t_{scan}) \qquad t > t_{scan} \tag{4b}$$

The following boundary conditions apply to the two problems of interest:

Potential step transients

microdisc electrode:

$$t = 0 \quad r \ge 0 \quad z \ge 0 \quad a = 1 \tag{5}$$

$$t > 0 \quad 0 \le r \le r_e \quad z = 0 \quad a = 0 \tag{6}$$

$$t > 0 \quad r > r_e \quad z = 0 \quad \partial a/\partial z = 0 \tag{7}$$

$$t > 0 \quad r \ge 0 \quad z \to \infty \quad a \to 1 \tag{8}$$

hemisphere electrode:

$$t = 0 \quad r \ge r_e \quad a = 1 \tag{9}$$

$$t > 0 \quad r = r_e \quad a = 0 \tag{10}$$

$$t > 0 \quad r \to \infty \quad a \to 1 \tag{11}$$

Cyclic voltammetry

microdisc electrode:

$$t = 0 \quad r \ge 0 \quad z \ge 0 \quad a = 1 \tag{12}$$

$$t > 0 \quad 0 \le r \le r_e \quad z = 0 \quad a = [1 + \exp(-\theta)]^{-1} \tag{13}$$

$$t > 0 \quad r > r_e \quad z = 0 \quad \partial a/\partial z = 0 \tag{14}$$

$$t > 0 \quad r \ge 0 \quad z \to \infty \quad a \to 1 \tag{15}$$

hemisphere electrode:

$$t = 0 \quad r \ge r_e \quad a = 1 \tag{16}$$

$$t > 0 \quad r = r_e \quad a = [1 + \exp(-\theta)]^{-1} \tag{17}$$

$$t > 0 \quad r \to \infty \quad a \to 1 \tag{18}$$

where r_e is the radius of the microdisc or microhemisphere electrode, the dimensionless potential, θ, is

$$\theta = \frac{F}{RT}(E^\circ - E) \tag{19}$$

and F is the Faraday constant. For either problem the current flowing at any instant may be deduced from

$$I = FD[\mathrm{A}]_{bulk} \int_0^{r_e} 2\pi r \left.\frac{\partial a}{\partial z}\right|_{z=0} \mathrm{d}r \tag{20}$$

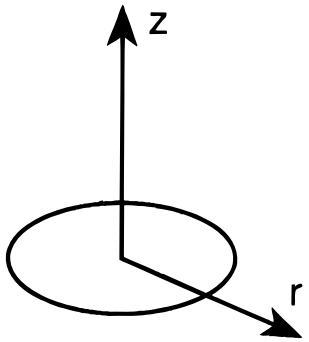

Figure 1. A microdisc electrode showing the cylindrical coordinate system.

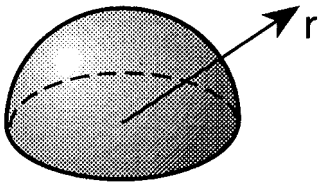

Figure 2. A hemispherical electrode showing the coordinate system.

for the case of a microdisc electrode, and from

$$I = FD[\mathrm{A}]_{bulk}\, 2\pi r_e^2 \left.\frac{\partial a}{\partial r}\right|_{r=r_e} \tag{21}$$

for a hemispherical electrode.

The problem of simulating transients at microdisc electrodes may be conveniently approached by means of the strongly implicit procedure,[23,24] and this was adopted to solve both the potential step and cyclic voltammetry problems defined above. In order to improve the accuracy and efficiency of the simulations, expanding r and z grids were used so that each of the coordinates were transformed using the functions[25]

$$R = \gamma_r \ln(1 + \epsilon_r r) \tag{22}$$

$$Z = \gamma_z \ln(1 + \epsilon_z z)$$

where

$$\gamma_r = \frac{1}{\ln(1 + r_e\epsilon_r)} \qquad \gamma_z = \frac{1}{\ln(1 + z_{max}\epsilon_z)} \tag{23}$$

The simulations were conducted on a rectangular region in the transformed space, which corresponds to a rectangle in real space: $0 \le r \le r_{max}$ and $0 \le z \le z_{max}$. ϵ_r and ϵ_z are grid expansion factors in the r and z coordinates.

The mass transport equation, in terms of the transformed coordinates, may be written as

$$\frac{\partial a}{\partial t} = D\left[\kappa_{Rd}\frac{\partial^2 a}{\partial R^2} + \kappa_{Rs}\frac{\partial a}{\partial R} + \kappa_{Zd}\frac{\partial^2 a}{\partial Z^2} + \kappa_{Zs}\frac{\partial a}{\partial Z}\right] \tag{24}$$

where

$$\kappa_{Zd} = \frac{\epsilon_z^2\gamma_z^2}{\exp(2Z/\gamma_z)} \qquad \kappa_{Rd} = \frac{\epsilon_r^2\gamma_r^2}{\exp(2R/\gamma_r)} \tag{25}$$

$$\kappa_{Zs} = -\frac{\epsilon_z^2\gamma_z}{\exp(2Z/\gamma_z)} \qquad \kappa_{Rs} = \frac{\epsilon_r \cdot \gamma_r}{1 + \epsilon_r r} - \frac{\epsilon_r^2\gamma_r}{\exp(2R/\gamma_r)}$$

Equation 24 may be cast into a finite difference form as

$$a_{j,k}^{t-1} = [-\lambda_{Rd} + \lambda_{Rs}]a_{j,k-l}^{t} + [-\lambda_{Zd} + \lambda_{Zs}]a_{j-l,k}^{t} + [1 + 2\lambda_{Rd} + 2\lambda_{Zd}]a_{j,k}^{t} + [-\lambda_{Zd} - \lambda_{Zs}]a_{j+l,k}^{t} + [-\lambda_{Rd} - \lambda_{Rs}]a_{j,k+l}^{t} \quad (26)$$

where

$$\lambda_{Rs} = \kappa_{Rs}\frac{D\Delta t}{2\Delta R} \qquad \lambda_{Zs} = \kappa_{Zs}\frac{D\Delta t}{2\Delta Z} \quad (27)$$

$$\lambda_{Rd} = \kappa_{Rd}\frac{D\Delta t}{(\Delta R)^2} \qquad \lambda_{Zd} = \kappa_{Zd}\frac{D\Delta t}{(\Delta Z)^2}$$

and $a_{j,k}^{t}$ denotes the concentration at finite difference node (j,k) with t denoting a time step counter. The finite difference form of eq 20 becomes

$$I = 2\pi FD[\mathrm{A}]_{\mathrm{bulk}}\frac{\epsilon_z\gamma_z}{\exp(Z/\gamma_z)}\frac{1}{\epsilon_r^{\,2}\gamma_r}\frac{\Delta R}{\Delta Z}\sum_{1}^{\mathrm{KE}}\{[\exp(k\Delta R/\gamma_r) - 1]\exp(k\Delta R/\gamma_r)\}a_{l,k} \quad (28)$$

where KE is the number of nodes across the electrode surface in the R coordinate, related to the total number of nodes in the R coordinate (NK), by

$$\mathrm{NK} = (\beta + 1)\mathrm{KE} \quad (29)$$

Hence the extent of the simulation space in the r coordinate, $r_{\max}$, is given by

$$r_{\max} = \frac{e^{(\beta+1)/\gamma_r} - 1}{\epsilon_r} \quad (30)$$

The SIP was otherwise implemented in the standard fashion,[24,26−28] and the interested reader is directed to the literature for the appropriate details.

For the case when B is kinetically unstable (forming C) the following mass transport equations hold:

$$\frac{\partial a}{\partial t} = D\frac{\partial^2 a}{\partial z^2} + D\frac{\partial^2 a}{\partial r^2} + \frac{D}{r}\frac{\partial a}{\partial r}$$

$$\frac{\partial b}{\partial t} = D\frac{\partial^2 b}{\partial z^2} + D\frac{\partial^2 b}{\partial r^2} + \frac{D}{r}\frac{\partial b}{\partial r} - k_n[\mathrm{A}]_{\mathrm{bulk}}^{n-1}b^n \quad (31)$$

$$\frac{\partial c}{\partial t} = D\frac{\partial^2 c}{\partial z^2} + D\frac{\partial^2 c}{\partial r^2} + \frac{D}{r}\frac{\partial c}{\partial r} + k_n[\mathrm{A}]_{\mathrm{bulk}}^{n-1}b^n$$

where $b = [\mathrm{B}]/[\mathrm{A}]_{\mathrm{bulk}}$, $c = [\mathrm{C}]/[\mathrm{A}]_{\mathrm{bulk}}$, n is 1 or 2 corresponding to an EC or EC_2 mechanism, and k_n is the corresponding rate constant. The initial concentrations (at $t = 0$) of both species B and C are, of course, zero. The simulation methods outlined above are directly applicable except rather than simulating just species A, two of the three species need to be simulated (the third can be readily calculated from mass conservation, provided all species have similar diffusion coefficients). Species B and C were simulated and the electrode surface boundary conditions were modified accordingly

$$\exp(\theta) = a_{0,k}^{t-1}/b_{0,k}^{t} \quad (32)$$

and

$$\left.\frac{\partial[\mathrm{C}]}{\partial z}\right|_{z=0} = 0 \quad (33)$$

so that species [B] and [C] could be solved sequentially (see the end of this section). The concentration of species A at the electrode surface can be calculated from:

$$[\mathrm{A}] = [\mathrm{A}]_{\mathrm{bulk}} - [\mathrm{B}] - n[\mathrm{C}] \quad (34)$$

The hemisphere electrode transients were simulated using the backwards implicit in time (BIT) method[27−30] applied in the standard manner described fully elsewhere.[27,28] Again the radial coordinate was transformed according to eq 22 so that the pertinent mass transport equation becomes

$$\frac{\partial a}{\partial t} = D\left[\kappa_{Rd}\frac{\partial^2 a}{\partial R^2} + \kappa_{Rsh}\frac{\partial a}{\partial R}\right] \quad (35)$$

where

$$\kappa_{Rsh} = \frac{2\epsilon r\gamma_r}{1 + \epsilon_r r} - \frac{\epsilon_r^{\,2}\gamma_r}{\exp(2R/\gamma_r)} \qquad \kappa_{Rd} = \frac{\epsilon_r^{\,2}\gamma_r^{\,2}}{\exp(2R/\gamma_r)} \quad (36)$$

This one-dimensional equation may be cast into finite difference form as

$$a_j^{t-1} = [-\lambda_{Rd} + \lambda_{Rsh}]a_{j-1}^{t} + [1 + 2\lambda_{Rd}]a_j^{t} + [-\lambda_{Rd} - \lambda_{Rsh}]a_{j+1}^{t} \quad (37)$$

where

$$\lambda_{Rsh} = \kappa_{Rsh}\frac{D\Delta t}{2\Delta R} \qquad \lambda_{Rd} = \kappa_{Rd}\frac{D\Delta t}{(\Delta R)^2} \quad (38)$$

which is readily solved using the BIT method.

For the case when species B is unstable (forming C) the pertinent mass transport equations are

$$\frac{\partial a}{\partial t} = D\frac{\partial^2 a}{\partial r^2} + \frac{2D}{r}\frac{\partial a}{\partial r} \quad (39)$$

$$\frac{\partial b}{\partial t} = D\frac{\partial^2 b}{\partial r^2} + \frac{2D}{r}\frac{\partial b}{\partial r} - k_n[\mathrm{A}]_{\mathrm{bulk}}^{n-1}b^n$$

$$\frac{\partial c}{\partial t} = D\frac{\partial^2 c}{\partial r^2} + \frac{2D}{r}\frac{\partial c}{\partial r} + k_n[\mathrm{A}]_{\mathrm{bulk}}^{n-1}b^n$$

The BIT method was used, with the radial coordinate transformation as above, to simulate species A and B simultaneously on a back-to-back grid (which is described elsewhere[31]) using the electrode boundary condition

$$\exp(\theta) = a_0^{t}/b_0^{t} \quad (40)$$

together with

$$\left.\frac{\partial a}{\partial r}\right|_{r=r_e} = -\left.\frac{\partial b}{\partial r}\right|_{r=r_e} \quad (41)$$

This allows the interrelated nodes of each species above the electrode surface to be expressed in terms of each other and thus species A and B to be solved simultaneously. The reason this method was not used for the transient microdisc simulations is that when applied to that system it gives rise to an off-diagonally dominant matrix, which causes the matrix equation solution algorithm to diverge.[32] Instead, the explicit electrode boundary condition (32) was used to decouple the species allowing them to be solved sequentially.

All programs were written in FORTRAN 77 using double precision (8 byte) variables, compiled with maximum optimization, and executed on Silicon Graphics Indigo^2 and Indy workstations.

Theory: Analytical Approaches

In this section we consider the expected dependence of the cyclic voltammogram in terms of the appropriate dimensionless variables.

Microdisc Electrode. The mass transport equation

$$\frac{\partial a}{\partial t} = D\frac{\partial^2 a}{\partial z^2} + D\frac{\partial^2 a}{\partial r^2} + \frac{D}{r}\frac{\partial a}{\partial r} \tag{42}$$

may be converted into a dimensionless form

$$\frac{\partial a}{\partial \tau} = \frac{\partial^2 a}{\partial \zeta^2} + \frac{\partial^2 a}{\partial \rho^2} + \frac{1}{\rho}\frac{\partial a}{\partial \rho} \tag{43}$$

where

$$\tau = Dt/r_e^2, \quad \rho = r/r_e, \quad \zeta = z/r_e \tag{44}$$

The electrode surface concentration is given in eq 13, and hence the concentration is a function of two space variables, a time variable, and the normalized potential (which itself is a function of time):

$$a = a(\tau,\zeta,\rho,\theta(t)) \tag{45}$$

Equation 4 may be rewritten in terms of dimensionless variables

$$\theta(\tau) = \theta_{init} + \nu\tau \tag{46}$$

where

$$\theta_{init} = \frac{F}{RT}(E_{init} - E^\circ) \qquad \nu = \frac{r_e^2}{D}\frac{Fs}{RT} \tag{47}$$

Hence the concentration is a function of four variables

$$a = a(\tau,\nu,\rho,\zeta) \tag{48}$$

The current is given by

$$I = Fa_{bulk}D\int_0^{r_e} 2\pi r \left.\frac{\partial a}{\partial z}\right|_{z=0} \mathrm{d}r \tag{49}$$

In terms of ρ and ζ this becomes

$$I = Fa_{bulk}\cdot 2\pi r_e D\int_0^1 \rho \left.\frac{\partial a}{\partial \zeta}\right|_{\zeta=0} \mathrm{d}\rho \tag{50}$$

Hence

$$I = Fa_{bulk}\cdot 2\pi r_e \mathrm{D} f_{disc}(\tau,\nu) \tag{51}$$

where f_{disc} denotes an unknown function which depends only on τ and ν.

Hemispherical Electrode. The mass transport equation

$$\frac{\partial a}{\partial t} = D\frac{\partial^2 a}{\partial r^2} + \frac{2D}{r}\frac{\partial a}{\partial r} \tag{52}$$

may be rewritten in term of dimensionless space and time variables

$$\frac{\partial a}{\partial \tau} = \frac{\partial^2 a}{\partial \rho^2} + \frac{2}{\rho}\frac{\partial a}{\partial \rho} \tag{53}$$

where

$$\tau = Dt/r_e^2 \qquad \rho = r/r_e \tag{54}$$

Considering the electrode surface concentration boundary given by eqs 45−47, as for the microdisc electrode

$$a = a(\tau,\nu,\rho) \tag{55}$$

The current is given by

$$I = Fa_{bulk}\cdot 2\pi r_e^2 D\left.\frac{\partial a}{\partial r}\right|_{r=r_e} \tag{56}$$

or in terms of ρ

$$I = Fa_{bulk}\cdot 2\pi r_e D\left.\frac{\partial a}{\partial \rho}\right|_{\rho=1} \tag{57}$$

Hence

$$I = Fa_{bulk}\cdot 2\pi r_e \mathrm{D} f_{hemi}(\tau,\nu) \tag{58}$$

where f_{hemi} denotes an unknown function which depends only on τ and ν.

Comparison of Microdisc and Hemisphere Peak Currents. At the peak of the cyclic voltammogram

$$\frac{\partial I}{\partial E} = \frac{\partial I}{\partial \theta} = 0 \tag{59}$$

The time dependence of the normalized potential is given by eq 46. Differentiating gives

$$\mathrm{d}\theta = \nu\,\mathrm{d}\tau \tag{60}$$

Hence the peak is also defined by

$$\partial I/\partial \tau = 0 \tag{61}$$

Applying this constraint to eq 51 for a microdisc gives

$$I_{peak}^{disc} = Fa_{bulk}\cdot 2\pi r_{disc} D f_{disc}(\nu_{disc}) \tag{62}$$

Similarly for the hemisphere, applying contraint (61) to eq 58 gives

$$I_{peak}^{hemi} = Fa_{bulk}\cdot 2\pi r_{hemi} D f_{hemi}(\nu_{hemi}) \tag{63}$$

The ratio of peak currents is therefore

$$\frac{I_{peak}^{hemi}}{I_{peak}^{disc}} = \frac{r_{hemi}}{r_{disc}} f_1(\nu_{disc},\nu_{hemi}) \tag{64}$$

From eq 47

$$\frac{r_{hemi}}{r_{disc}} = \sqrt{\frac{\nu_{hemi}}{\nu_{disc}}} \tag{65}$$

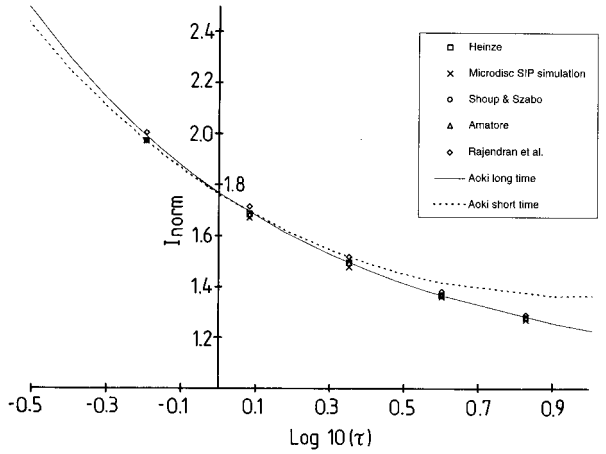

Figure 3. Comparison of analytical and simulated dimensionless current-time transients at a microdisc electrode. $I_{norm} = I/FDw[A]_{bulk}$. Parameters for the SIP simulation are shown in Table 1.

TABLE 1: Parameters Used in the Simulation of Potential Step Transients at a Microdisc

electrode radius	r_{disc} (μm)	1
diffusion coeff	D (cm^2 s^{-1})	2×10^{-5}
bulk concn	$[A]_{bulk}$ (mol cm^{-3})	1×10^{-6}
simulation space outside electrode radius	β	2.3
simulation space above electrode	z_{max} (μm)	7.5
simulation time	t_{sim} (ms)	0.4
time steps per second	NT	40 000 000
no. of nodes in r direction	NK	300
no. of nodes in z direction	NJ	300
grid expansion factor in r direction	ϵ_r	10 000
grid expansion factor in z direction	ϵ_z	10 000
SIP acceleration parameter	APARAM	30
SIP convergence threshold: residual errors	CONRES	1×10^{-6}
SIP convergence threshold: change in residual errors	CONCHN	1×10^{-5}

Hence

$$\frac{I_{peak}^{hemi}}{I_{peak}^{disc}} = f_2(\nu_{disc},\nu_{hemi}) \qquad (66)$$

where f_1 and f_2 denote unknown functions.

Results and Discussion

Potential Step Transients. In order to assess the veracity of the SIP modeling procedure, the simulation of potential step transients was compared with data published by other workers. Simulations were first conducted for microdisc electrodes using the parameters given in Table 1. Figure 3 shows the results plotted in dimensionless form together with the simulations of (i) Heinze,[33] obtained using the ADI method, (ii) Shoup and Szabo,[34] whom employed the Hopscotch method, and (iii) Amatore,[8] who used a conformal map with the Hopscotch method. In addition, the analytical expressions derived by Aoki[35,36] for long and short time limits are shown, as is an equation derived by Rajendran and Sangaranarayanan.[37] All the simulations show good mutual agreement and tend between the two limits obtained by Aoki while the values predicted by Rajendran and Sangaranarayanan appear a little high in comparison, on average by ca. 1.1% in the range shown in Figure 3. The results shown in Figure 3 are highly satisfactory and indicate the successful implementation of the SIP in the simulation of transient microdisc mass transport problems.

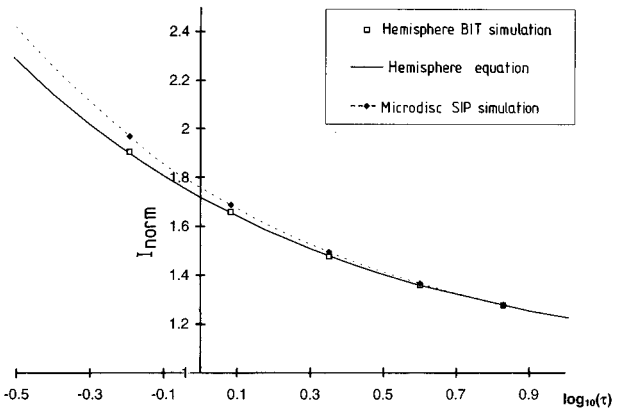

Figure 4. Comparison of analytical and simulated dimensionless current−time transients at a hemispherical electrode to a simulated dimensionless current−time transient at a microdisc electrode. I_{norm} is as defined in Figure 2. Parameters for the BIT simulation are shown in Table 2.

TABLE 2: Parameters Used in the Simulation of Potential Step Transients at a Hemisphere

electrode radius	r_{hemi} (μm)	0.637
diffusion coeff	D (cm^2 s^{-1})	2×10^5
bulk concn	$[A]_{bulk}$ (mol cm^{-3})	1×10^{-6}
simulation space outside electrode radius	r_{max}	$12r_{hemi}$
simulation time	t_{sim} (ms)	1
time steps per second	NT	4 000 000
no. of nodes in r direction	NJ	6000
grid expansion factor in r direction	ϵ_r	1 000 000

Next, attention was switched to the simulation of potential step transients resulting at microhemisphere electrodes. Table 2 shows the parameters used in the BIT simulations and the results are shown in Figure 4, together with the corresponding analytical expression for a hemisphere:

$$I = 2\pi r_{hemi}{}^2 FD[A]_{bulk}\left[\frac{1}{\sqrt{\pi Dt}} + \frac{1}{r_{hemi}}\right] \qquad (67)$$

The simulation can be seen to agree very well with analytical theory. Figure 4 also shows a comparison of the potential step transients of a microdisc electrode of radius r_{disc} (as above) and a hemispherical electrode of radius:

$$r_{hemi} = 2r_{disc}/\pi \qquad (68)$$

A comparable response is predicted[12−14] for the two electrodes under steady-state conditions. As can be seen from Figure 4, the microdisc current tends to that of the hemispherical electrode at long times. Pictorially, this corresponds to when the microdisc diffusion layer, initially approximately planar, tends to hemispherical in shape. This evolution is shown in Figure 5.

All the potential step results validate the SIP simulation method employed under transient conditions, showing it to be in excellent agreement with other simulations on microdisc electrodes.[7−11,33−40] Next, therefore, we simulate cyclic voltammetry by modification of the electrode boundary condition, confident in the ability of SIP to deliver quantitatively correct transient simulation data.

Cyclic Voltammetry at a Hemispherical Microelectrode. Simulations were conducted using the BIT method together, for purposes of comparison, with the commercial one-dimensional cyclic voltammetry package DigiSim. The parameters employed in these simulations are given in Table 3. Table 4 gives a comparison between the results of the two ap-

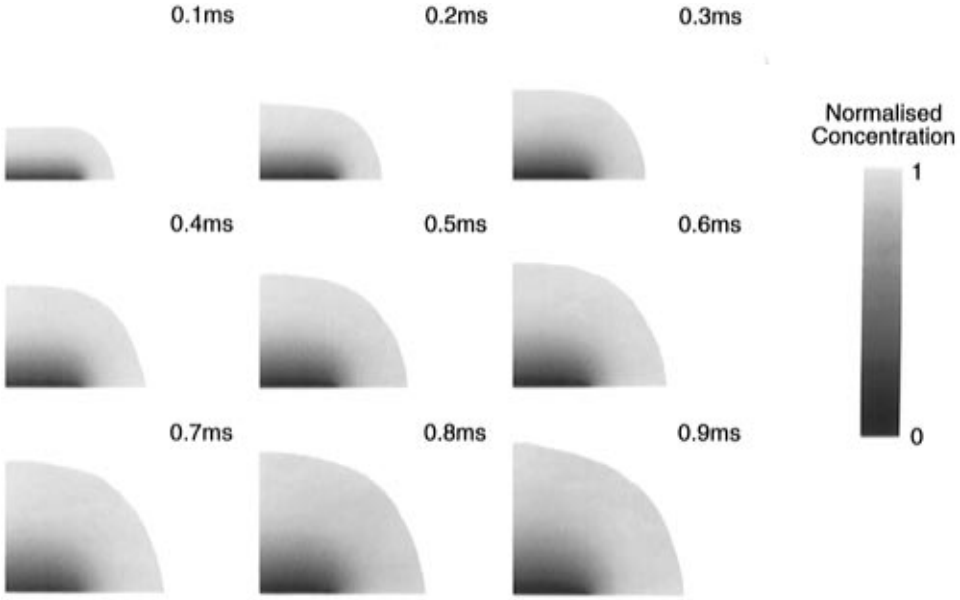

Figure 5. Concentration profile evolution at a microdisc electrode after a potential step. Parameters are NJ = 100, NK = 100, $\beta = 0.75$, $z_{max} = 0.001$ cm, $\epsilon_r = 10\,000$, $\epsilon_z = 10\,000$, NT = 400 000, Simt = 1 ms, $r_{disc} = 0.0004$ cm, $D = 2 \times 10^{-5}$ cm^2 s^{-1}, $[A]_{bulk} = 1 \times 10^{-6}$ cm^{-3} s^{-1}. Concentration profiles are shown at 0.1 ms intervals. 5/6 of the simulation space is shown in each direction.

TABLE 3: Parameters Used in the Simulation of Cyclic Voltammograms at a Hemisphere

scan rate (V s^{-1})	s	100	200	500	1000	2000
electrode radius (μm)	r_{hemi}	0.637	0.637	0.637	0.637	0.637
diffusion coeff (cm^2 s^{-1})	D	2×10^{-5}	2×10^{-5}	2×10^{-5}	2×10^{-5}	2×10^{-5}
bulk concn (mol cm^{-3})	$[A]_{bulk}$	1×10^{-6}	1×10^{-6}	1×10^{-6}	1×10^{-6}	1×10^{-6}
simulation space outside electrode radius	r_{max}	12r	12r	20r	20r	12r
simulation time (ms)	t_{sim}	20	10	4	2	1
time steps per second	NT	200 000	200 000	1 000 000	1 000 000	1 000 000
no. of nodes in r direction	NJ	6000	6000	6000	6000	6000
grid expansion factor in r direction	ϵ_r	1 000 000	1 000 000	1 000 000	1 000 000	1 000 000

TABLE 4: A Comparison of Simulation Methods for Hemispherical Electrodes

	hemisphere BIT simulation		DigiSim (hemisphere)		planar eqn
scan rate (V s^{-1})	I_{peak} (A)	peak separation (V)	I_{peak} (A)	peak separation (V)	I_{peak} (A)
100	9.83×10^{-10}	0.143	9.81×10^{-10}	0.146	9.81×10^{-10}
200	1.09×10^{-9}	0.122	1.09×10^{-9}	0.124	1.09×10^{-9}
500	1.32×10^{-9}	0.102	1.32×10^{-9}	0.103	1.32×10^{-9}
1000	1.59×10^{-9}	0.095	1.59×10^{-9}	0.091	1.59×10^{-9}
2000	1.98×10^{-9}	0.081	1.98×10^{-9}	0.082	1.99×10^{-9}

proaches: data is shown at five scan rates, for the peak currents and peak-to-peak separation (in volts). The agreement between the two simulation methods is excellent. Also shown are the peak currents predicted by the classical analytical cyclic voltammetry theory of Shain and Nicholson[41] incorporating their "spherical correction":

$$I = FA[A]_{bulk}\sqrt{\pi D\sigma}\chi(\sigma t) + \frac{FDA[A]_{bulk}\phi(\sigma t)}{r_{hemi}} \quad (69)$$

where A is the area of the hemispherical electrode, r_{hemi} is the radius of the hemisphere, and σ is defined as

$$\sigma = Fs/RT \quad (70)$$

Values of the functions ϕ and χ have been tabulated.[41] Again the agreement is excellent.

Cyclic Voltammetry at a Microdisc Electrode. SIP simulations were conducted for the microdisc geometry using the parameters shown in Table 5. The results may be compared with the results of the BIT hemisphere simulations reported in Tables 3 and 4. Figure 6 shows the corresponding pairs of voltammograms at scan rates of 100, 200, 500, 1000, and 2000 V s^{-1} for a microdisc and a microhemisphere electrodes of radius 1 and 0.637 μm, respectively. The steady-state currents compare well in agreement with theoretical prediction.[42,43] However, inspection shows that the peak currents deviate from each other with the peak current of the microdisc electrode increasing relatively more above that of the hemispherical electrode with increasing scan rate. This is illustrated by Figure 7 which shows a plot of peak current vs scan rate for a microdisc electrode of radius 1 μm, a "planar" electrode using the data from Table 6, and an "equivalent" hemispherical electrode of radius 0.637 μm using the data from Table 4. The data for the planar electrode was generated using DigiSim and from the analytical expression:[41]

$$I = FA[A]_{bulk}\sqrt{\pi D\sigma}\chi(\sigma t) \quad (71)$$

where A is the area of the planar electrode and the other symbols are as for eq 69.

The current passed at the microdisc is clearly enhanced over both of the other cases where one-dimensional diffusion operates; this is attributable to edge effects contributing significantly to the net current. Figure 7 further emphasizes

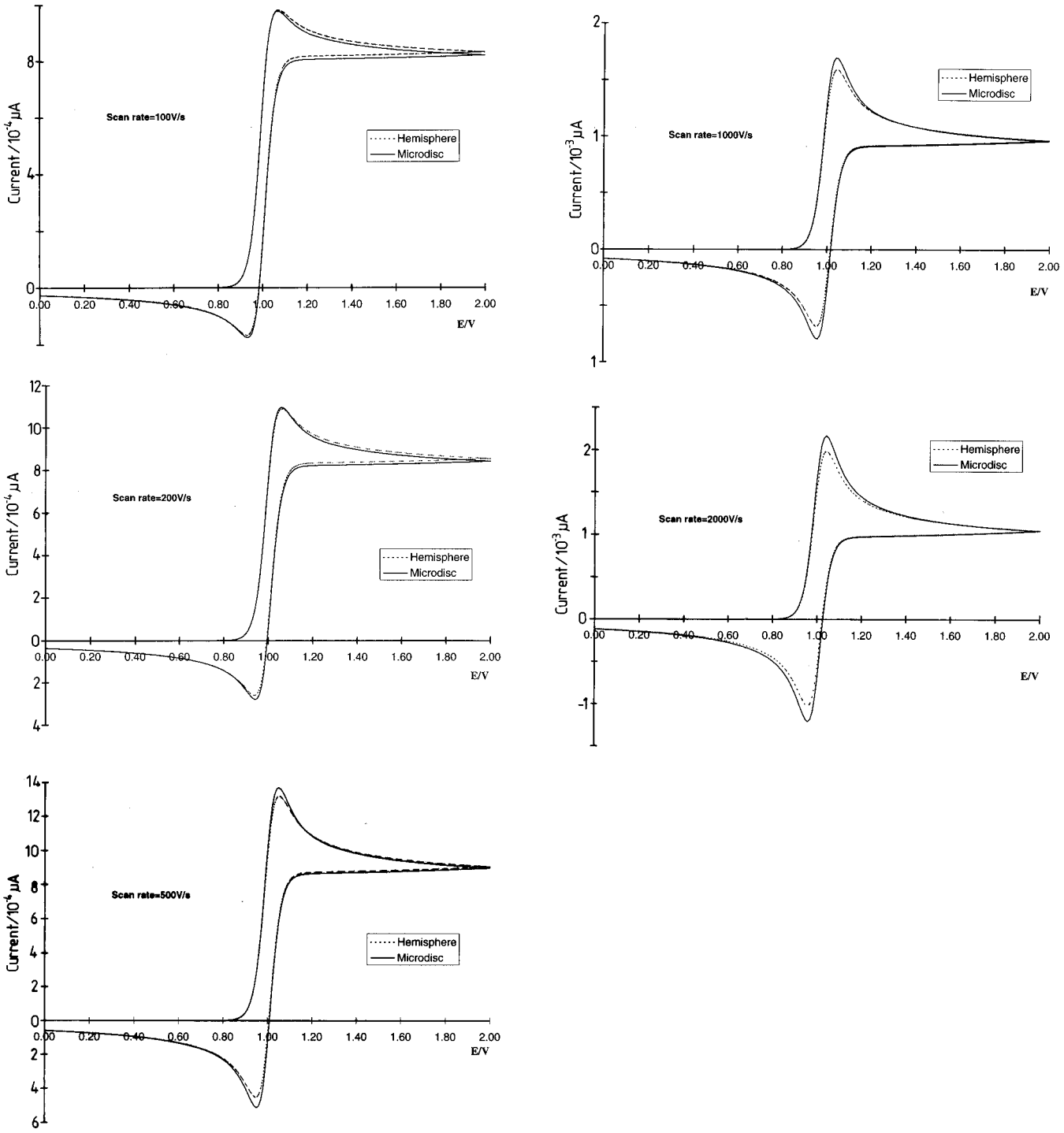

Figure 6. Comparison of cyclic voltammograms at a microdisc and hemispherical electrode for five scan rates. Parameters for the BIT and SIP simulations are shown in Tables 3 and 5.

TABLE 5: Parameters Used in the Simulation of Cyclic Voltammograms at a Microdisc

scan rate (V s^{-1})		100	200	500	1000	2000
electrode radius (μm)	r_{disc}	1	1	1	1	1
diffusion coeff (cm^2 s^{-1})	D	2×10^{-5}	2×10^{-5}	2×10^{-5}	2×10^{-5}	2×10^{-5}
bulk concn (mol cm^{-3})	$[A]_{bulk}$	1×10^{-6}	1×10^{-6}	1×10^{-6}	1×10^{-6}	1×10^{-6}
simulation space outside electrode radius	β	4	4	3.5	3.0	2.3
simulation space above electrode (μm)	z_{max}	50	50	20	10	7.5
simulation time (ms)	t_{sim}	40	20	8	4	2
time steps per second	NT	10,000	20,000	50,000	100,000	200,000
no. of nodes in r, coordinate	NK	300	300	300	300	300
no. of nodes in z coordinate	NJ	300	300	300	300	300
grid expansion factor in r coordinate	ϵ_r	10000	10000	10000	10000	10000
grid expansion factor in z coordinate	ϵ_z	10000	10000	10000	10000	10000
SIP acceleration parameter	APARAM	30	30	30	30	30
SIP convergence threshold: residual errors	CONRES	1×10^{-6}	1×10^{-6}	1×10^{-6}	1×10^{-6}	1×10^{-6}
SIP convergence threshold: change in residual errors	CONCHN	1×10^{-5}	1×10^{-5}	1×10^{-5}	1×10^{-5}	1×10^{-5}

TABLE 6: A Comparison of Simulation Methods for Microdisc Electrodes

	microdisc SIP simulation		DigiSim (planar)		planar eqn	
scan rate (V s^{-1})	I_{peak} (A)	peak separation (V)	I_{peak} (A)	peak separation (V)	I_{peak} (A)	peak separation (V)
100	9.79×10^{-10}	0.140	3.77×10^{-10}	0.0578	3.78×10^{-10}	0.057
200	1.10×10^{-9}	0.120	5.34×10^{-10}	0.0578	5.35×10^{-10}	0.057
500	1.37×10^{-9}	0.096	8.44×10^{-10}	0.0578	8.45×10^{-10}	0.057
1000	1.70×10^{-9}	0.080	1.19×10^{-9}	0.0578	1.20×10^{-9}	0.057
2000	2.17×10^{-9}	0.080	1.69×10^{-9}	0.0578	1.69×10^{-9}	0.057

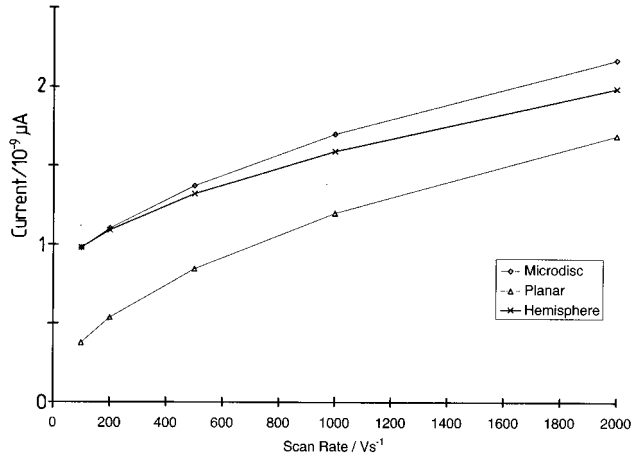

Figure 7. Comparison of peak currents at a microdisc, hemispherical and a planar electrode, using the data in Tables 4 and 6.

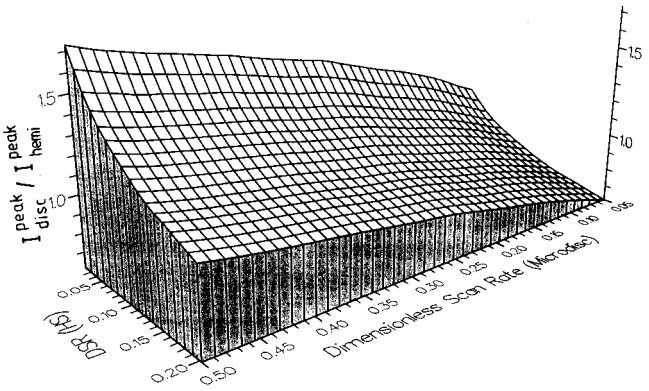

Figure 8. Working surface for hemisphere/disc peak current ratios.

the increasing departure of the microdisc peak current from that of the "equivalent" hemisphere with increasing scan rate. *Figures 6 and 7 emphasize the dangers in treating the cyclic voltammetric response of a microdisc electrode by the equivalent hemipshere approximation.*

The comparison of the microdisc and microhemisphere may be generalized by means of the conclusions drawn in a preceding section of this paper in which it is shown that the ratio of the microdisc to hemisphere peak currents is a unique function of the corresponding two dimensionless scan rates. Figure 8 shows a partial working surface in which the ratio $I_{disc}^{peak}/I_{hemi}^{peak}$ is plotted as a function of ν_{disc} and ν_{hemi}. *The deviation of the disc and hemisphere behavior is again evident and signals necessary caution in using the latter theory to interpret results from the former geometry. This caveat may be particularly relevant if experimental results over a range of different scan rates are to be considered, since the deviation increases with scan rate.*

Cyclic Voltammetry and Coupled Homogeneous Kinetics. The ultimate aim of most cyclic voltammetric investigations is the deduction of the mechanism and associated kinetic parameters. Accordingly, simulations were run for both EC and EC_2 reactions. Higher values of NT (corresponding to 16 000 time steps) were used to ensure the solution remained converged at high rate constants because of the explicit electrode boundary condition.

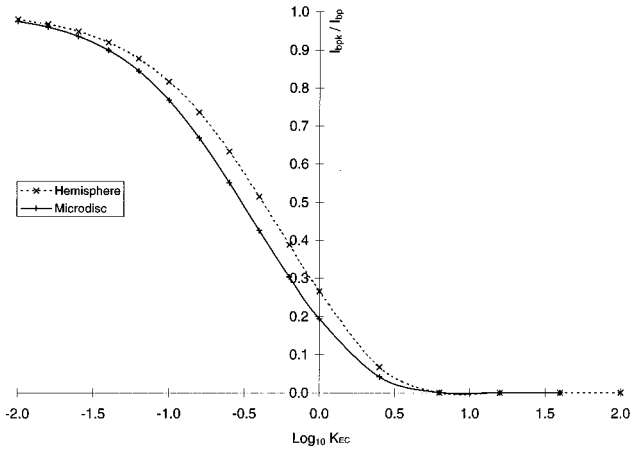

Figure 9. Ratio of the back peak current with EC kinetics to that in the absence of homogeneous kinetics plotted as a function of the dimensionless rate constant at a dimensionless scan rate of 10. For the microdisc simulation, NT = 2.05×10^6 (corresponding to 16 000 time steps) $\beta = 3.5$, $z_{max} = 20$ μm. For the hemisphere 8000 time steps were used, $r_{max} = 60 r_{hemi}$. All other parameters are as in Tables 3 and 5.

In the presence of homogeneous kinetics, the process is characterized by a diminuation of the "back" cyclic voltammetric peak relative to the forward peak as the rate constant characterizing the homogeneous chemistry increases relative to the rate of mass transport. Experimentally, this is accomplished by slowing the voltage scan rate, *s*. The key observable relating theory and experiment is therefore the magnitude of the current corresponding to the reconversion of B to A relative to the corresponding current seen when B is stable. Figure 9 shows the results of simulations for an EC process at a 1 μm disc electrode with a dimensionless scan rate of $\nu_{disc} = 10$ (corresponding to a real scan rate of 513.56 V s^{-1}) and an equivalent hemisphere electrode of radius 0.637 μm. The ratio of the back peak current relative to the no-kinetics case is plotted as a function of the dimensionless rate constant

$$K_{EC_n} = \frac{k_n r_{disc}^{\ 2} [A]_{bulk}^{n-1}}{D} \qquad (72)$$

where *k* is the rate constant (mol^{-1-n} $cm^{3(n-1)}$ s^{-1}) characterizing the homogeneous chemistry of interest. It can be seen that the back current decreases as K_{EC} gets larger, as expected, but that the simulated responses for hemisphere and disc electrodes are quite different. If ν_{disc} is increased to 100 then Figure 10 shows that, as anticipated, the deviation between one- and two-dimensional transport becomes more exaggerated. Figures 11 and 12 show the corresponding exercise for EC_2 processes. Again deviation from the simple one-dimensional case is seen at the fastest scan rate although the discrepancies are less than for the EC mechanism. This reflects the key difference between disc and hemisphere electrodes in that for a simple electrode

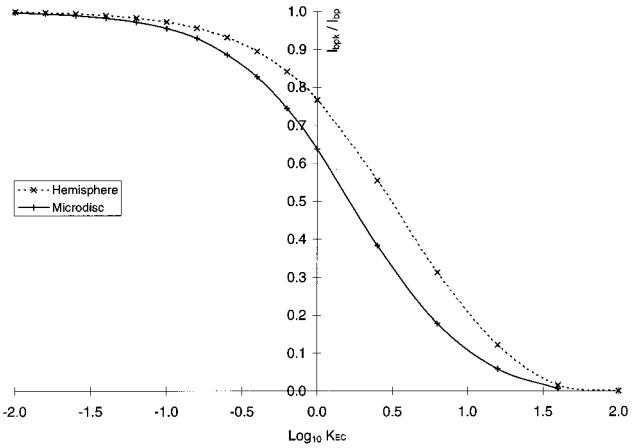

Figure 10. The analog of Figure 9 at a dimensionless scan rate of 100. For the microdisc simulation, NT = 2.05×10^7 (corresponding to 16 000 time steps), $\beta = 2.0$, $z_{max} = 4\ \mu$m. For the hemisphere 8000 time steps were used, $r_{max} = 60 r_{hemi}$. All other parameters are as in Tables 3 and 5.

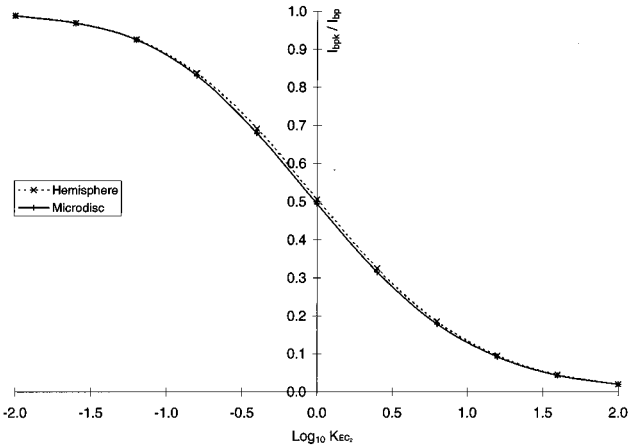

Figure 11. Ratio of the back peak current with EC_2 kinetics to that in the absence of homogeneous kinetics plotted as a function of the dimensionless rate constant at a dimensionless scan rate of 10. Parameters are as for Figure 9.

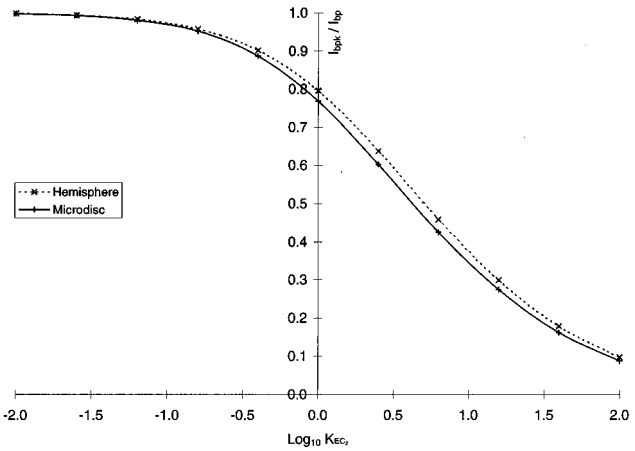

Figure 12. The analog of Figure 9 at a dimensionless scan rate of 100. Parameters are as for Figure 10.

process with no kinetics, the nonuniformity of the former leads to a build up of B in the center as compared to the periphery of the disc unlike the latter where the distributions of A and B are uniform around the electrode. When B is unstable the concentration of B is reduced. For an EC_2 process this has the effect of returning the concentration profile to being relatively more uniform whereas for an simple EC reaction the concentration is diminished proportionately. Nevertheless, as shown by Figure 12 *even at modest scan rates the disc/hemisphere analogy is compromised.*

Conclusions

Cyclic voltammetry at a microdisc electrode may be successfully simulated using the SIP. The results, in agreement with previous studies,[7−11] confirm that under steady-state conditions the response of a microdisc of radius r_{disc} corresponds to that of a hemisphere of radius $2r_{disc}/\pi$. However, as emphasized by Figure 8, even at modest scan rates at a small microdisc there is a significant deviation in the cyclic voltammetric response. This is particularly significant if the electrode process embraces homogeneous chemistry as illustrated in Figures 10 and 12. We conclude that the potentially popular approximation of one-dimensional transport for microdisc problems should be adopted with due caution. The unthinking use of DigiSim and analogous software to apply planar or hemisphere diffusion models to microdisc electrodes may embarass.

Acknowledgment. We thank the EPSRC for a studentship for J.A.A.

References and Notes

(1) Fleischmann, M.; Pons, S. *Ultramicroelectrodes*; Datatech: Morgantown, NC, 1987.
(2) Wang, J. *Microelectrodes*; VCH: New York, 1990.
(3) Montenegro, M. I. *Res. Chem. Kinet.* **1994**, *2*, 1.
(4) Amatore, C. A.; Lefrou, C. *Port. Electrochim. Acta* **1991**, *9*, 311.
(5) Amatore, C. A.; Jutand, A.; Pfluger, F. *J. Electroanal. Chem.* **1987**, *218*, 361.
(6) Heinze, J.; Störzbach, M. *Ber. Bunsenges. Phys. Chem.* **1986**, *90*, 1043.
(7) Micheal, A. C.; Wightman, R. M.; Amatore, C. A. *J. Electroanal. Chem.* **1989**, *267*, 33.
(8) Amatore, C. R.; Fosset, B. *J. Electroanal. Chem.* **1992**, *328*, 21.
(9) Mirkin, M. V.; Bard, A. J. *J. Electroanal. Chem.* **1992**, *323*, 1.
(10) Taylor, G.; Girault, H. H.; McAleer, J. *J. Electroanal. Chem.* **1990**, *293*, 19.
(11) Verbrugge, M. W.; Baker, D. R. *J. Phys. Chem.* **1992**, *96*, 4572.
(12) Oldham, K. B. *J. Electroanal. Chem.* **1981**, *122*, 1.
(13) Tutty, O. R. *J. Electroanal. Chem.* **1994**, *377*, 39.
(14) Phillips, C. G. *J. Electroanal. Chem.* **1990**, *296*, 255.
(15) Fleischmann, M.; Lasserre, F.; Robinson, J.; Swan, D. *J. Electroanal. Chem.* **1984**, *177*, 97.
(16) Fleischmann, M.; Lasserre, F.; Robinson, J. *J. Electroanal. Chem.* **1984**, *177*, 115.
(17) Denuault, G.; Mirkin, M. V.; Bard, A. J. *J. Electroanal. Chem.* **1991**, *308*, 27.
(18) DigiSim is a registered trademark of Bioanalytical Systems, Inc.
(19) Rudolph, M.; Reddy, D. P.; Feldberg, S. W. *Anal. Chem.* **1994**, *66*, 589A.
(20) Rudolph, M. *Electroanal. Chem.* **1991**, *314*, 13.
(21) Rudolph, M. *Electroanal. Chem.* **1992**, *338*, 85.
(22) Aoki, K.; Akimoto, K.; Tokuda, K.; Matsuda, H.; Osteryoung, J. *J. Electroanal. Chem.* **1984**, *171*, 219.
(23) Stone, H. L. *SIAM J. Numer. Anal.* **1968**, *5*, 530.
(24) Alden, J. A.; Compton, R. G.; Dryfe, R. A. W. *J. Appl. Electrochem.* **1996**, *26*, 865.
(25) Feldberg, S. W. *J. Electroanal. Chem.* **1981**, *127*, 1.
(26) Compton, R. G.; Dryfe, R. A. W.; Wellington, R. G.; Hirst, J. *J. Electroanal. Chem.* **1995**, *383*, 13.
(27) Alden, J. A.; Compton, R. G. *J. Electroanal. Chem.* **1996**, *402*, 10.
(28) Alden, J. A.; Compton, R. G.; Dryfe, R. A. W. *J. Electroanal. Chem.* **1995**, *397*, 11.
(29) Anderson, J. L.; Moldoveanu, S. *J. Electroanal. Chem.* **1984**, *179*, 107.
(30) Laasonen, P. *Acta Math.* **1949**, *81*, 30917.
(31) Bidwell, M. J.; Alden, J. A.; Compton, R. G. *J. Electroanal. Chem.* **1996**, *417*, 119.

(32) Alden, J. A.; Compton, R. G. *J. Electroanal. Chem.* **1996**, *415*, 1.
(33) Heinze, J. *J. Electroanal. Chem.* **1981**, *124*, 73.
(34) Shoup, D.; Szabo, A. *J. Electroanal. Chem.* **1982**, *140*, 237.
(35) Aoki, K.; Tokuda, K.; Matsuda, H. *Denki Kagaku* **1986**, *54*, 1010.
(36) Aoki, K.; Tokuda, K.; Matsuda, H. *J. Electroanal. Chem.* **1987**, *230*, 61.
(37) Rajendran, L.; Sangaranarayanan, M. V. *J. Electroanal. Chem.* **1995**, *392*, 75.
(38) Britz, D. *J. Electroanal. Chem.* **1996**, *406*, 15.
(39) Denuault, G.; Mirkin, M. V.; Bard, A. J. *J. Electroanal. Chem.* **1991**, *308*, 27.
(40) Fleischmann, M.; Pletcher, D.; Denuault, G.; Daschbach, J.; Pons, S. *J. Electroanal. Chem.* **1989**, *263*, 225.
(41) Nicolson, R. S.; Shain, J. *Anal. Chem.* **1964**, *36*, 706.
(42) Newman, J. *J. Electrochem. Soc.* **1966**, *113*, 501.
(43) Gröber, H. *Die Grundgesetze der Warmeleitung und des Wärmeüberganges*; Springer: Berlin, 1921.